Title

Effects of aging and environmental tobacco smoke exposure on ocular and plasma circulatory microRNAs in the Rhesus macaque.

Authors

Smit-McBride, Zeljka
Nguyen, Johnny
Elliott, Garrett W
et al.

Publication Date

2018

Peer reviewed

Molecular Vision 2018; 24:633-646 <http://www.molvis.org/molvis/v24/633>
Received 26 February 2018 | Accepted 21 September 2018 | Published 24 September 2018

Effects of aging and environmental tobacco smoke exposure on ocular and plasma circulatory microRNAs in the Rhesus macaque

Zeljka Smit-McBride,[1] Johnny Nguyen,[1] Garrett W. Elliott,[1] Zhe Wang,[2] Ryan A. McBride,[3] Anthony T. Nguyen,[1] Sharon L. Oltjen,[1] Glenn Yiu,[1] Sara M. Thomasy,[1,4] Kent E. Pinkerton,[5,6] Eugene S. Lee,[7] David Cunefare,[8] Sina Farsiu,[8,9] Lawrence S. Morse[1]

[1]Department of Ophthalmology & Vision Science, School of Medicine, University of California, Davis, Davis, CA; [2]School of Veterinary Medicine, University of California, Davis, Davis, CA; [3]Department of Cell Biology and Human Anatomy, School of Medicine, University of California, Davis, Davis, CA; [4]Department of Surgical and Radiological Sciences, School of Veterinary Medicine, University of California, Davis, Davis, CA; [5]California National Primate Research Center, University of California, Davis, Davis, CA; [6]Center for Health & the Environment (CHE), University of California, Davis, Davis, CA; [7]Sacramento VA Medical Center, Mather, CA; [8]Department of Biomedical Engineering, Duke University, Durham, NC; [9]Department of Ophthalmology, Duke University, Durham, NC

Purpose: To identify changes induced by environmental tobacco smoke (ETS) in circulatory microRNA (miRNA) in plasma and ocular fluids of the Rhesus macaque and compare these changes to normal age-related changes. Tobacco smoke has been identified as the leading environmental risk factor for age-related macular degeneration (AMD).
Methods: All Rhesus macaques were housed at the California National Primate Research Center (CNPRC), University of California, Davis. Four groups of animals were used: Group 1 (1–3 years old), Group 2 (19–28 years old), Group 3 (10–16 years old), and Group 4 (middle aged, 9–14 years old). Group 4 was exposed to smoke for 1 month. Ocular fluids and plasma samples were collected, miRNAs isolated, and expression data obtained using Affymetrix miRNA GeneTitan Array Plates 4.0. Bioinformatics analysis was done on the Affymetrix Expression Console (EC), Transcriptome Analysis Software (TAS) using ANOVA for candidate miRNA selection, followed by Ingenuity Pathway Analysis (IPA).
Results: The expression of circulatory miRNAs showed statistically significant changes with age and ETS. In the plasma samples, 45 miRNAs were strongly upregulated (fold change >±1.5, $p<0.05$) upon ETS exposure. In the vitreous, three miRNAs were statistically significantly downregulated with ETS, and two of them (miR-6794 and miR-6790) were also statistically significantly downregulated with age. Some retinal layers exhibited a thinning trend measured with optical coherence tomography (OCT) imaging. The pathways activated were IL-17A, VEGF, and recruitment of eosinophils, Th2 lymphocytes, and macrophages.
Conclusions: ETS exposure of Rhesus macaques resulted in statistically significant changes in the expression of the circulatory miRNAs, distinct from those affected by aging. The pathways activated appear to be common for ETS and AMD pathogenesis. These data will be used to develop an animal model of early dry AMD.

Age-related macular degeneration (AMD) is the most common form of visual impairment in elderly individuals in the Western world. AMD is a complex blinding disease, affected by genetic and environmental factors, as well as epigenetic regulators. Cigarette smoke is the leading environmental risk factor, second only to aging. Recently, a central regulatory role for a novel type of epigenetic regulator, miRNA, has been discovered in many human diseases. MiRNAs are considered master regulatory switches, playing roles in numerous health and disease processes, as well as in aging and epigenetics. Some miRNAs can be induced in response to environmental challenges, thus allowing the organism to modify its underlying genetic programming in response to a changing environment.

Although knowledge about miRNAs and their function is accumulating rapidly, knowledge specific to their role in healthy ocular aging and age-related pathologies of the eye is lacking. In this project, we used tobacco smoke exposure as a model of a common environmental insult that affects ocular tissue. Smoke-induced damage is mediated in part through direct oxidation, depletion of antioxidants, complement activation, and inflammation [1]. Interestingly, similar processes have been shown to be critical in the pathology of AMD. Although research in recent years has identified some mechanisms of AMD pathogenesis, this research is limited by the lack of appropriate animal models for AMD. The most commonly used model is the rodent which lacks macula and never truly develops hallmark lesions of AMD, such as drusen. Although primates develop an age-related

Correspondence to: Zeljka Smit-McBride, Department of Ophthalmology & Vision Science, Vitreoretinal Research Lab, School of Medicine, University of California, Davis, Davis, CA 95616, One Shields Ave, Tupper Hall #2403, Phone: (530)320-8474, FAX: (530) 752-2270; email: zsmcbride@ucdavis.edu

maculopathy that is equivalent to human AMD [2], this process takes decades, which is impractical for an experimental approach.

Our long-term goal is to develop a primate model of retinal degeneration, which would resemble AMD. Given that cigarette smoke, or more encompassing, environmental tobacco smoke (ETS) exposure, is the leading environmental risk factor for AMD, second only to aging, we hypothesize that there is a common mechanism between ETS-induced damage and AMD pathogenesis. We hypothesize that miRNAs regulate normal age-related homeostatic processes in the retina. Therefore, the purpose of this study was to identify the initial changes that occur in circulatory miRNA in the ocular fluids and plasma during normal aging and compare the changes to the changes that occur with ETS exposure. We identified differentially expressed miRNAs in plasma and ocular fluids during normal, healthy aging and determined that process was considerably different compared to pathologic changes induced by an environmental insult, modeled by short-term exposure to tobacco smoke. Interestingly, some of the pathways activated with ETS were the same as those involved in AMD pathogenesis.

METHODS

Animals: Rhesus macaques used for this study were housed at the California National Primate Research Center (CNPRC) at University of California, Davis. There were four experimental groups of female animals (a total of 16 animals): Group 1 (young, 1–3 years; n=4), Group 2 (old, 19–28 years; n=5), Group 3 (middle aged, 10–16; n=3), and Group 4 (middle aged, 9–14; n=4). The Group 4 was exposed to smoke for 1 month at the CNPRC facility (Appendix 1). All procedures conformed to the ARVO Statement for the Use of Animals in Ophthalmic and Vision Research. These procedures were also authorized by the Institutional Animal Care and Use Committee (#18988) at the University of California, Davis.

Clinical assessment of animals: Rhesus macaques selected for the ETS exposure experiment were clinically assessed and found healthy in the absence of (n=6) or following (n=4) ETS exposure. Fundus photography using the CF-1 retinal camera (Canon, Tokyo, Japan) and spectral domain optical coherence tomography (SD-OCT) imaging were performed using the Spectralis device (Heidelberg Engineering, Heidelberg, Germany) as detailed below.

Spectral domain OCT Imaging: SD-OCT imaging was performed using the Spectralis SD-OCT device (Heidelberg Engineering), which had been modified with a flat chin-rest to allow the Rhesus monkeys' heads to be positioned. OCT images were captured with a 30° × 5° SD-OCT raster scan with 1536 A-scans per B-scan and 234 µm of spacing between B-scans. This was performed in the high-resolution mode with 25 scans averaged for each B-scan using the device's eye-tracking capability. Images were semiautomatically segmented using the Duke Optical Coherence Tomography Retinal Analysis Program (DOCTRAP, version 62.0), custom image analysis software designed using MATLAB (Mathworks) [3]. Segmentation boundaries were automatically calculated by DOCTRAP using graph-based determination of reflectivity profiles and then manually refined by the two graders. Thickness measurements were averaged across the 3 mm segment centered on the fovea in each horizontal line-scan, and included the nerve fiber layer (NFL), ganglion cell layer (GCL), inner plexiform layer (IPL), inner nuclear layer (INL), outer plexiform layer (OPL), outer nuclear layer (ONL), photoreceptor inner segments (IS), photoreceptor outer segments (OS), retinal pigment epithelium (RPE), choriocapillaris (CC), and choroid (C). Total retinal thickness was measured from the internal limiting membrane (ILM) to Bruch's membrane (BM).

Statistical analysis: All measurements reported in this study were calculated using the average measurements from two graders. The mixed-effect ANOVA was performed to test the pre/post exposure effects on all retinal layers. A mixed-design ANOVA model (also known as a split-plot ANOVA) is used to test for differences between two or more independent groups while subjecting participants to repeated measures. Differences in chorioretinal layer thicknesses obtained from the SD-OCT pre/post exposure were compared using a mixed-effect ANOVA, with two independent variables: The within-subject factor variable was pre/post exposure and eyes [oculus sinister (OS) / oculus dextrus (OD)] while the between-subject factor variable was an animal ID. The dependent variable was the thickness of each layer. All statistical analysis was performed using SPSS software (version 22, IBM). The segmentation analysis and quantification of the retinal layers are shown for the total retinal thickness measurement along the central 3 mm region for all four animals. The mean value of retinal layer thickness was calculated for each layer in four monkeys pre/post exposure. No statistical significance was found for pre/post exposure eyes.

Tobacco smoke exposure study design: Groups 1 through 3 were housed in standard indoor animal housing, while Group 4 was housed in standard caging in a modified animal holding room specifically designed for ETS. Tobacco smoke exposure occurred over 4 weeks with ETS delivered for approximately 6 h per day, 5 days a week. The exposure room was ventilated with filtered air during non-ETS exposure periods or with ETS diluted with filtered air during exposure periods.

Necropsies were performed on the day immediately following the last exposure day.

Tobacco smoke exposure study analyses:

Carbon monoxide (CO)—A Teledyne-API Model 300E Carbon Monoxide (CO) Analyzer (Teledyne Instruments, San Diego, CA) was used to continuously monitor the CO concentration in the exposure room for the duration of the exposure. Data were acquired in parts per million (ppm) every 4 min.

Nicotine—Two samples were collected per day, for 1 h each. Tobacco smoke–exposed air was drawn through a stainless steel sample tube at a flow rate of 2,000 ml/min for 1 h through an XAD-4 sorbent tube, which was sealed after sample collection and stored in the refrigerator. Nicotine samples were analyzed by the UC Davis Center for Health and the Environment (CHE) as previously described [4].

Total mass concentration—Tobacco smoke–exposed air was drawn through a stainless steel sample tube at a flow rate of 2,000 ml/min for 1 h. The sample was collected on a Pallflex® 25 mm Fiberfilm filter (Pall Corp., East Hills, NY), which was weighed on a Sartorius Model MC5 microbalance before and after sampling.

Cotinine assays—Blood samples were collected in 7 ml EDTA vacutainer tubes for the control animals and at 15- and 30-day time points in the ETS-exposed animals. A cotinine ELISA kit was purchased from Calbiotech (Spring Valley, CA), and samples were assayed according to the manufacturer's protocol.

Tissue collection: Ocular fluid samples were collected when the animals were euthanized. Blood samples were collected at the beginning of the experiment and when the animals were euthanized. Animals were euthanized following the standard CNPRC protocol: the animal was sedated with Ketamine at a dosage of 10 mg/kg. After that sodium pentobarbital greater or equal to 120 mg/kg Fatal Plus or Beuthanasia Plus 1 ml/4.5 kg was administered intravenously to the animal for euthanasia. After each animal was euthanized, 100–200 µl samples of aqueous and vitreous humor and 10 ml of venous blood for plasma were collected. Plasma was isolated using ACCUSPIN tubes (MilliporeSigma, St. Louis, MO) following the manufacturer's protocol. Plasma samples were stored at −80 °C.

Ocular tissue fixation and hematoxylin-eosin staining: Enucleated eyes were immersion fixed overnight at room temperature in 2% phosphate-buffered paraformaldehyde containing 0.5% glutaraldehyde, pH 7.4 (0.1 M phosphate buffer). After overnight fixation, the eyes were bisected, the lens removed, and the bisected eye was placed in 4% phosphate-buffered formalin for approximately 1 week to reverse glutaraldehyde fixation before embedding in paraffin. The eyes were embedded in paraffin as follows: washed in PBS (1X; 154 mM NaCl, 1.1 mM KH_2PO_4, 5.6 mM Na_2HP0_4, pH 7.4), dehydrated through graded ethanol washes (50%, 75%, 95%, and 100% ethanol), and gradually cleared in xylene using a step-wise procedure (2:1 ethanol to xylene; 1:1 ethanol to xylene; 1:2 ethanol to xylene), followed by xylene before embedding in paraffin. Sections were cut (6 µm) using a Leica RM2125RT microtome (Leica, Nussloch, Germany), placed on SuperFrost Plus microscope slides, and dried overnight at room temperature. Standard hematoxylin-eosin staining was performed on the sectioned eyes.

RNA isolation: All the samples were collected within a 1 h after the animals were euthanized, processed immediately, and stored in aliquots at −80 °C until RNA isolation. The total RNA, which included miRNAs, was isolated from each of the individual samples using miRCURY™ RNA Isolation Kits -Biofluids (Qiagen, Germantown, MD). A small aliquot of the sample was frozen separately for quantification and quality control on BioAnalyzer, so the main sample tube was thawed only once during the process of labeling probe for GeneChip microarray hybridization. Total isolated RNA (5–10 ng/µl) from fluid samples was analyzed using the BioAnalyzer using Small RNA Analysis Kit (Agilent Technologies, Santa Clara, CA) following the manufacturer's protocol.

Probe labeling for hybridization to microRNA microarrays: MiRNA samples (20 ng) were labeled as probes, using the FlashTag kit (ThermoFisher Scientific, Waltham, MA) following the manufacturer's protocol and hybridized to microRNA microarrays. Two Affymetrix miRNA microarrays GeneTitan Plates 4.0, each with 24 samples, for a total of 48 samples, were run at the UCSF Institute for Human Genetics (IHG). Raw data in the form of probe cell intensity data (.cel) files were retrieved and subjected to bioinformatics analysis.

Bioinformatics analysis: Probe cell intensity data (.cel) from Affymetrix GeneChip® miRNA Arrays were analyzed with the Affymetrix® Expression Console (EC) software (ThermoFisher Scientific). The application uses the RMA + DABG analysis for doing background subtraction, normalization, and summarization of the probe sets from Affymetrix expression microarrays, and the final output is a .chp file. Spearman rank order correlation coefficients between biologic replicates were computed by EC to assess the between samples correlations (Appendix 2). Generated .chp files for each sample were imported into Affymetrix Transcriptome Analysis Console (TAC; ThermoFisher Scientific) for subsequent analysis of differentially expressed genes.

Table 1. Tobacco smoke exposure data of Rhesus macaques.

Statistical categories	Carbon monoxide ppm	Total mass Conc. [mg/m^3]	Nicotine [mg/m^3]
Mean	24.44	1.89	0.61
STD Dev	1.27	0.19	0.09
Minimum	17.82	1.42	0.42
Maximum	26.53	2.15	0.84
Sample Size	1424	20	40
Total No. Cigarettes Smoked:	7780		

Statistical analysis of microarray data—The criteria used to determine a statistically significant change in miRNA abundance was −1.5 ≥ fold change (FC) ≥1.5, p≤0.05. ANOVA was used for calculating the statistical significance and identifying the p values for each microRNA. The data were filtered for *Macaca mulatta* (Rhesus macaque).

Ingenuity pathway analysis—Ingenuity Pathway Analysis software (Qiagen) was used for gene pathway analysis and the identification of potential miRNA gene targets. Raw data were deposited at NCBI Gene Expression Omnibus (GEO), Accession Number GSE108951.

Quantitative polymerase chain reaction (qPCR) assays: Real-time qPCR assays (TaqMan assays, ThermoFisher Scientific) were run on miRNA isolated from plasma samples for ETS versus control on three replicas for each group and in triplicate for each replica. Assays were run at the Real-time PCR Research and Diagnostics Core Facility at UC Davis. Each miRNA sample was amplified using a TaqMan preamplification procedure and TaqMan preamp primers (Applied Biosystems, Life Technologies, Grand Island, NY) following manufacturers protocols. Reverse transcription thermal-cycling conditions were: 16 °C/30 min, 42 °C /30 min, 85 °C /5 min, hold 4 °C /∞. Pre-amplification thermal-cycling conditions were: 95 °C /10 min, 55 °C /2 min, 72 °C /2 min, 95 °C /15 s, 12 cycles of 95 °C /15 s, 60 °C /4 min, hold at 99.9 °C /10 min, hold 4 °C /∞. The samples were run in 384 well plates. Real-time thermal-cycling conditions: hold 95 °C /10 min, 40 cycles of 95 °C /15 sec, 60 °C /60 s, hold 4°C /∞. The TaqMan assays performed were miR-221 (ABI No. 000524, hsa-miR-221), miR-26a (ABI No. 000405, hsa-miR-26a), let-7c-5p (ABI No. 000379, hsa-let-7c), and three control genes, miR-486-5p (ABI No. 001278, hsa-miR-486), miR-320b (ABI No. 002844, hsa-miR-320b), and miR-638 (ABI No. 001582, hsa-miR-638). MiRNA assays were conducted at a dilution of 1:100s, and each run was done in triplicate. A control with no enzyme in the reverse transcriptase (RT) step was included as a negative control.

RESULTS

Tobacco smoke exposure: The adult female Rhesus macaques in Group 4 (exposure) received four 7-day cycles of 1.42–2.15 mg/m^3 of tobacco smoke for an average of 6 h/day on days 1–5, followed by 2 days in the filtered air (Table 1). During exposure, filtered air ventilation was lowered to 3.5 room air exchanges per hour. The daily average nicotine level of exposure measured through XAD-4 sorbent tubes was (0.610 mg/m^3 ±0.090). In animals that underwent ETS exposure, ocular health was evaluated by veterinary and physician ophthalmologists (SMT and GY) pre- and post-exposure. The control group (Group 3) was housed in standard indoor animal housing.

Cotinine results: Cotinine is an alkaloid found in tobacco and is the predominant metabolite of nicotine [5]. Cotinine concentrations in the control and ETS-exposed animals at day 30 are displayed in Table 2. On average, ETS-exposed animals contained statistically significantly higher (p<0.01), concentrations of cotinine compared to control animals at the 15-day time point (48.6±13.1 ng/ml versus 0 ng/ml) and the 30-day time point (54.9±5.0 ng/ml versus 0.06±.001 ng/ml).

Table 2. Plasma cotinine concentrations of Rhesus macaques - 15 and 30 day time points.

Time point	Cotinine concentration	
	Controls	TS exposed animals
15 days	0 ng/ml	48.6±13.1 ng/ml
30 days	0.06±.001 ng/ml	54.9±5.0 ng/ml

Clinical evaluations of ETS-exposed macaques: Rhesus macaques from Groups 3 and 4 were clinically assessed before and following ETS exposure. Ophthalmic examinations did not identify any visible ocular changes pre- and post-exposure (Figure 1). Retinal imaging, performed using OCT, followed by segmentation analysis and quantification of the retinal layers is shown for the total retinal thickness measurement along the central 3 mm region for all four animals (Table 3). There were trends noted in the thinning of the nuclear fiber layer (NFL; 17.36±0.860 um versus 16.01±0.470 um ($p<0.17$) and in the thickening of the choriocapillaris layer (CC; 18.60±2.050 versus 19.46±2.240 ($p<0.34$), pre- and post-ETS exposure, although these trends were not statistically significant.

Small RNA profiles from plasma and aqueous and vitreous humor: Representative profiles from the BioAnalyzer small RNA kit are shown in Figure 2. There was an abundance of circulatory miRNA molecules in each of the fluids analyzed. Representation of miRNA in each of the fluid compartments isolated from 200 µl of fluid was within the range of 2.30–14.6 ng/µl in the aqueous, 0.8–2.2 ng/µl in the vitreous, and 0.16–0.32 ng/µl in the plasma. The small RNA bands were abundant (Figure 2, red arrow) and the range of the sizes of the small RNA molecules was comparable to the range in the profile of the high-quality small RNA fraction in the solid tissue RNA prep (data not shown). The total concentration of miRNA in nanograms/microliters did not change statistically significantly in the plasma samples from the same animals pre- and post-exposure.

The total number of miRNAs detected: In the plasma samples, 40 microRNAs were ubiquitously present ($p<0.05$) in all samples, and up to 204 variably. In vitreous, ten miRNAs were ubiquitously present in all samples and up to 88 variably, and in aqueous, seven were ubiquitously present and up to 148 variably. The presence of microRNAs was established according to the Affymetrix P/A/M detection algorithm based on the Wilcox signed-rank test introduced by Affymetrix [6].

Changes in primate circulatory miRNA expression after ETS exposure: In the plasma samples, 45 miRNAs were statistically significantly upregulated after ETS exposure (Figure 3A). In the vitreous samples, three miRNAs were statistically significantly downregulated after ETS exposure (Figure 3B). There were no statistically significantly dysregulated miRNAs observed in the aqueous samples. All miRNAs with their fold change and p-values ($-1.5 \geq FC \geq 1.5$; $p<0.05$) are listed in Appendix 3, Appendix 4, Appendix 5, Appendix 6, Appendix 7.

Age-related changes in circulatory miRNAs: In the plasma samples from the aging monkeys, two miRNAs were statistically significantly downregulated between old (Group 2) versus young (Group 1) macaques (Figure 4). In the vitreous and aqueous samples, six miRNAs were statistically significantly downregulated in each compartment ($-1.5 \geq FC \geq 1.5$; $p<0.05$). All dysregulated miRNAs differed between the vitreous and aqueous samples.

Validation of microarray results with qPCR: Independent quantitative PCR (qPCR) validation of representative differentially expressed genes was performed using commercial gene expression assays (TaqMan; Applied Biosystems), following manufacturers protocol (for detailed reaction conditions see Materials and Methods section on Quantitative polymerase chain reaction (qPCR) assays). The fold changes and their direction were confirmed for the chosen sets of genes. Data are presented in Table 4.

Pathway analysis of miRNAs differentially regulated after ETS exposure: Ingenuity Pathway Analysis identified two top networks that are activated during ETS exposure: IL-17A and VEGF. One of the top IPA pathways that incorporates the activation of both networks is the inflammatory pathway of recruitment and activation of eosinophils, Th2 lymphocytes, and macrophages (Figure 5).

DISCUSSION

In addition to a role in cardiovascular and cerebrovascular diseases, as well as a host of cancers, tobacco smoking is the principal risk factor for AMD in the industrialized world. The genetics of AMD has been well studied with several risk alleles identified, such as those found in *CFH* (Gene ID: 3075, OMIM 134370) and *HTRA1* (Gene ID: 5654, OMIM 610149) [7,8]. However, environmental factors, which are easily modifiable and potentially could prevent or mitigate AMD, are understudied. Thus, there is an increasing urgency to understand the mechanisms involved in ETS pathogenesis, particularly given the proliferation of new forms of nicotine delivery [9-11].

Primate ETS exposure levels were within the range of strong environmental tobacco smoke exposure: Curtis's and other groups have shown that 1 month of high ETS exposure produces chronic obstructive pulmonary disease (COPD) in primate animal models [12,13]. Our working hypothesis was that the retina and the choroid, highly vascular tissues that are sensitive to oxidative stress, might be similarly impacted by short-term ETS exposure. Furthermore, environmental second-hand smoke has been shown to have serious health effects [14-16]. We measured animal exposure to ETS using several criteria: particulate matter, nicotine, and cotinine. Cotinine is an alkaloid found in tobacco and the predominant metabolite of nicotine [5]. Cotinine has an in vivo half-life

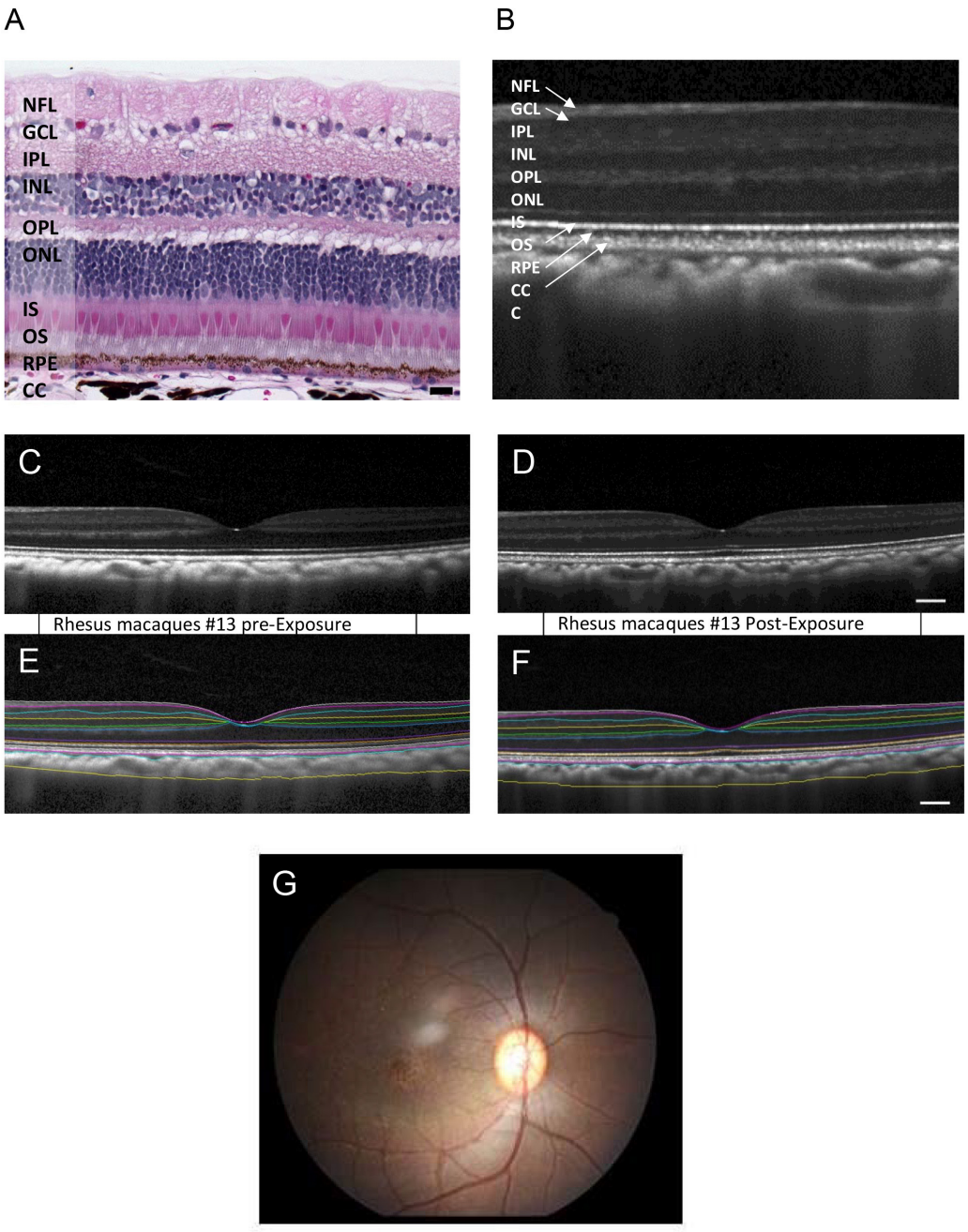

Figure 1. Imaging of the Rhesus macaque eye pre- and post-cigarette smoke exposure. **A**: Hematoxylin and eosin (H&E) staining showing Rhesus macaque retina layers. **B**: Representative spectral domain optical coherence tomography (SD-OCT) image using the enhanced depth imaging (EDI) mode to optimize visualization of the choroid, showing comparable retinal layers. **C**: SD-OCT image of the Rhesus macaque fovea region before smoke exposure. **D**: SD-OCT of the same eye post-exposure. Digital image segmentation of the same eye preexposure performed on the line scan closest to the foveal center, defined as the center of the foveal pit with the greatest separation between the IS/OS junction and the RPE layer. **E**: Digital images of SD-OCT images were semiautomatically segmented using the Duke Optical Coherence Tomography Retinal Analysis Program (DOCTRAP, version 62.0), a custom image analysis software designed using MATLAB (Mathworks). **F**: Digital image segmentation of the same eye post-exposure. **G**: Fundus image of the Rhesus macaque eye. NFL, Nerve fiber layer; GCL, Ganglion cell layer; IPL, Inner plexiform layer; INL, Inner nuclear layer; OPL, Outer plexiform layer; ONL, Outer nuclear layer; IS, Photoreceptor inner segments; OS, Photoreceptor outer segments; RPE, Retinal pigment epithelium; CC, Choriocapillaris; C, Choroid.

Table 3. Comparison of chorioretinal thicknesses of Rhesus macaque eye measured by Spectral Domain OCT Imaging (SD-OCT) pre- and post- ETS exposure.

Retinal layers	Pre-exposure (um)	Post-exposure (um)	P value
Nerve fiber layer (NFL)	17.36±0.86	16.01±0.47	0.17
Ganglion cell layer (GCL)	23.60±1.54	24.35±1.81	0.6
Inner plexiform layer (IPL)	34.32±1.59	33.75±1.29	0.77
Inner nuclear layer (INL)	29.95±1.59	30.58±1.34	0.37
Outer plexiform layer (OPL)	22.20±0.88	22.26±0.74	0.95
Outer nuclear layer (ONL)	85.30±2.59	85.31±2.94	0.98
Photoreceptor inner segments (IS)	23.66±1.03	23.20±0.85	0.68
Photoreceptor outer segments (OS)	45.12±1.85	44.60±1.33	0.73
Retinal pigment epithelium (RPE)	24.14±1.38	25.23±1.71	0.49
Choriocapillaris (CC)	18.60±2.05	19.46±2.24	0.34
Choroid (C)	179.57±8.27	177.44±13.90	0.89
All layers	305.64±6.74	305.28±6.98	0.82

The differences have not reached statistical significance at $p<0.05$, although NFL layer ($p<0.17$) showed the most substantial change in Pre/Post-exposure thickness.

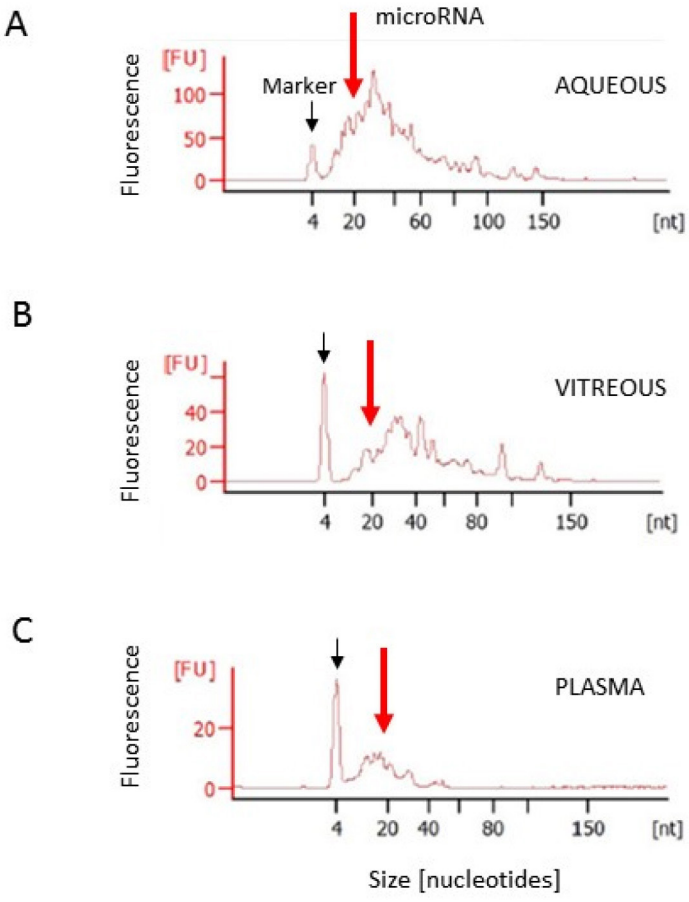

Figure 2. Comparison of BioAnalyzer RNA profiles of circulatory microRNAs and small RNAs in Rhesus macaque ocular fluids and plasma. RNA profiles have the front labeled with a fluorescent marker (black arrow) and microRNA peak (red arrow): aqueous humor (**A**), vitreous humor (**B**), and plasma (**C**).

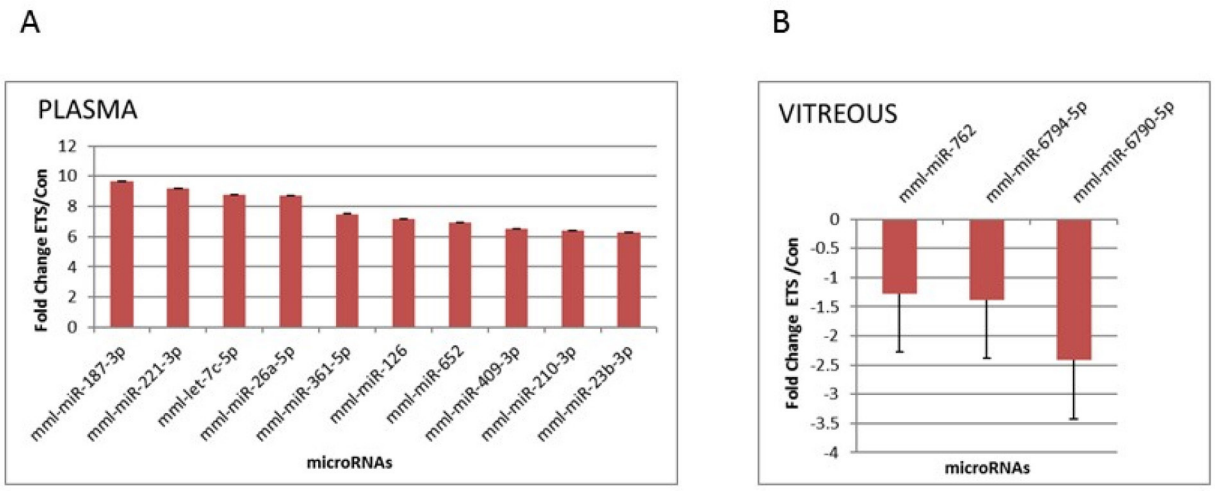

Figure 3. Differential expression of circulatory microRNAs in Rhesus macaques exposed to ETS, compared to controls. Data are presented as fold change (FC) values (−1.5 ≥ FC ≥ 1.5; p<0.05) in the plasma (ETS: n=4, control: n=4; top ten; **A**) and the vitreous (ETS: n=4, control: n=2; **B**). Error bars represent the standard deviation (SD) between the samples.

of approximately 20 h and is typically detectable up to 1 week after the use of tobacco. The amounts of cotinine in blood, saliva, and urine are proportionate to the amount of exposure to tobacco smoke; thus, cotinine is a valuable indicator of tobacco smoke exposure, including secondary (passive) smoke [17]. The nicotine concentrations measured in the current study were consistent with second-hand smoke exposure, and the cotinine assays confirmed marked ETS exposure with a concentration of about 50 ng/ml. In humans, cotinine concentrations of about 30 ng/ml indicate marked exposure [18].

The thickness of retinal layers did not change statistically significantly following ETS exposure, which was consistent with the literature on humans: All macaques were clinically assessed before and following ETS exposure. Fundus photography of the back of the eye did not show any visible changes pre- or post-exposure. Retinal imaging using OCT, followed by segmentation analysis and quantification of the retinal layers, showed no statistical significance in the total retinal thickness or any of the retinal layers. This result was consistent with findings in human smokers, where the central macular thickness shows no statistically significant differences between smokers and non-smokers [19,20]. Although not reaching a statistical significance level, perhaps because of the small animal numbers and only 1 month of exposure, a trend in the thinning of the NFL was observed. This observation is consistent with the literature showing that smoking tobacco may cause considerable thinning of the NFL in heavy smokers [20-22]. In addition, we observed the trend of choriocapillaris thickening in primates exposed to ETS. This result is consistent with the findings that exposure to ETS results in the formation of sub-RPE deposits, thickening of Bruch's membrane, and the accumulation of deposits within Bruch's membrane. All these processes lead to an injury stimulus of the choriocapillaris and RPE, which may explain the association between tobacco smoking and early AMD [23]. One of the limitations of this study is that the OCT-based measurements are limited by the inclusion of Henle's fiber layer within the ONL rather than the OPL to which the layer belongs [24]. Thus, true longitudinal changes in the OPL at the macula may not be accurate.

Circulatory miRNA changes in response to ETS exposure were different from those that occur during the normal aging process: Upon ETS exposure, the greatest changes in circulatory miRNAs were observed in the plasma (45 miRNAs were strongly upregulated), followed by the vitreous (three miRNAs were downregulated). However, there were no statistically significantly dysregulated miRNAs detected in the aqueous humor. These results differ markedly from what occurs during normal aging where only two miRNAs were statistically significantly downregulated in the plasma, while in the vitreous and aqueous six different miRNAs were statistically significantly downregulated (-1.5>FC>1.5; p<0.05). The only exceptions, two out of three novel miRNAs identified as downregulated following ETS exposure in the vitreous (miR-6794 and miR-6790) were the same ones observed to be downregulated in the vitreous during normal aging.

Dysregulated miRNAs common to ETS exposure and AMD: Circulating miRNAs are excellent biomarkers. They can be

Table 4. Comparison of results (Fold Change) from microarrays and qPCR miRNA expression from pre- and post- ETS exposure plasma samples of Rhesus macaques.

miRBase ID	Accession number	Fold change	ANOVA	Fold change	qPCR
		microarray	P value	qPCR	t
mml-miR-221–3p	MIMAT0002583	9.17	0.0004*	5.97	0.08
mml-miR-26a-5p	MIMAT0002349	8.72	0.007*	4.66	0.11
mml-let-7c-5p	MIMAT0006153	8.76	0.003*	3.38	0.07

ANOVA is reported for microarray data, while *t* test (1-tailed, paired) is reported for qPCR data. The fold change values for microarray data are all statistically significant at p<0.01 (marked with *). Fold change values for qPCR data are not statistically significant at p<0.05, although they are approaching significance.

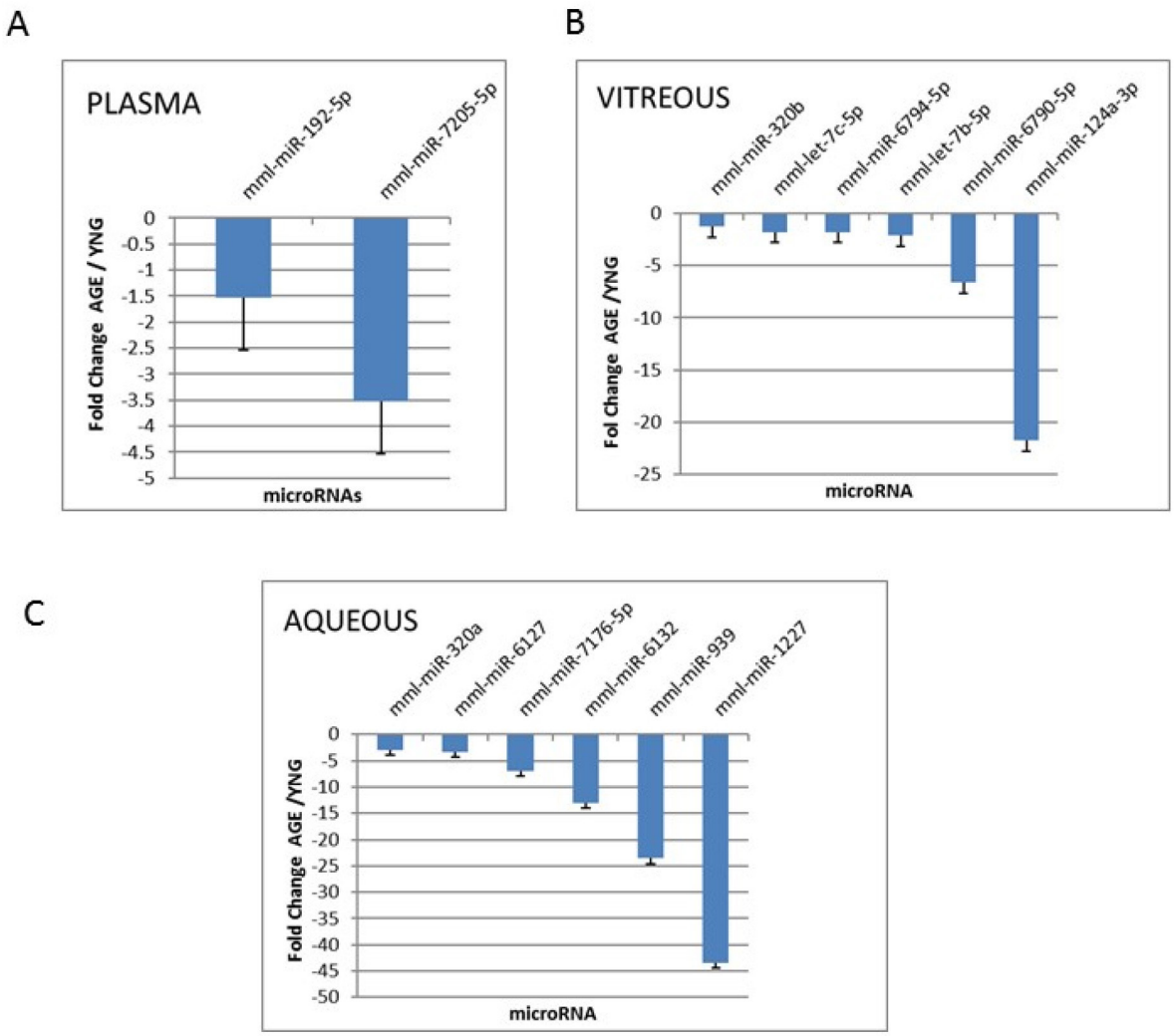

Figure 4. Differential expression of circulatory microRNAs in old compared to young Rhesus macaques. Data are presented as fold change (FC) values (−1.5 ≥ FC ≥ 1.5; p<0.05) of the old animals compared to young animals in the plasma (young: n=4, old: n=4; **A**), vitreous (young: n=4, old: n=3; **B**), and aqueous (young: n=4, old: n=4; **C**). Error bars represent the standard deviation (SD) between the replicate samples.

easily sampled from plasma and bodily fluids, including ocular fluids, thus gaining the name of the liquid biomarker or liquid biopsy [25]. They are stable for hours, even at room temperature, because they travel protected associated with proteins or encapsulated by small vesicles called exosomes [26].

In addition to being accessible biomarkers, miRNAs are biologically powerful molecules that regulate

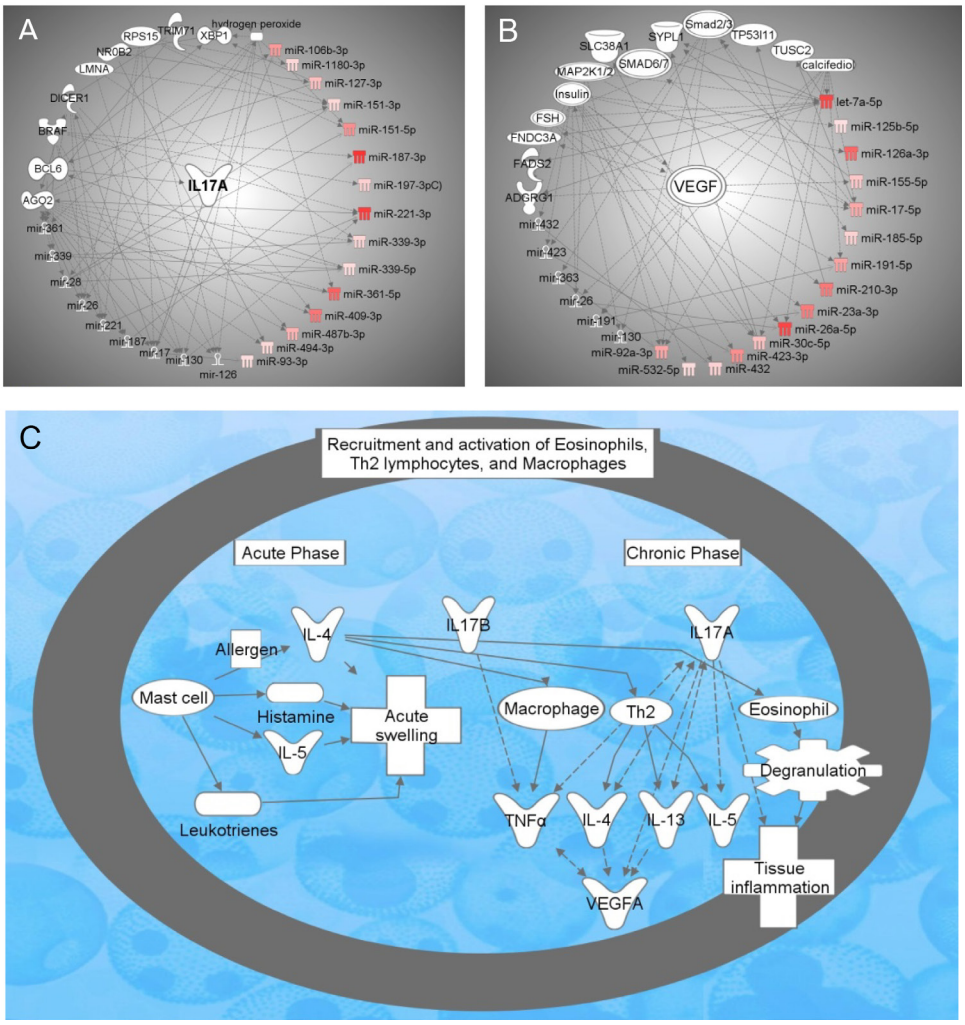

Figure 5. Pathway Analysis of the smoke-induced microRNAs and their target genes. **A**: MicroRNAs and gene network targeting IL-17A: AGO2 (argonaute 2, RISC catalytic component); BCL6 (B-cell CLL/lymphoma 6); BRAF (B-Raf proto-oncogene, serine/threonine kinase); DICER1 (dicer 1, RNase III); IL-17A (interleukin-17A); LMNA (lamin A/C); miR-106b-3p (miRNAs w/seed CGCACUG); miR-1180-3p (miRNAs w/seed UUCCGGC); mir-126; miR-127-3p (miRNAs w/seed CGGAUCC); mir-130; miR-151-3p (and other miRNAs w/seed UAGACUG); miR-151-5p (and other miRNAs w/seed CGAGGAG); mir-17; mir-187; miR-187-3p (miRNAs w/seed CGUGUCU); miR-197-3p (and other miRNAs w/seed UCACCAC); mir-221; miR-221-3p (and other miRNAs w/seed GCUACAU); mir-26; mir-28; mir-339; miR-339-3p (miRNAs w/seed GAGCGCC); miR-339-5p (and other miRNAs w/seed CCCUGUC); mir-361; miR-361-5p (miRNAs w/seed UAUCAGA); miR-409-3p (miRNAs w/seed AAUGUUG); miR-487b-3p (miRNAs w/seed AUCGUAC); miR-494-3p (miRNAs w/seed GAAACAU); miR-93-3p (miRNAs w/seed CUGCUGA); NR0B2 (nuclear receptor subfamily 0 group B member 2); RPS15 (ribosomal protein S15); TRIM71 (tripartite motif containing 71); XBP1 (X-box binding protein 1). **B**: MicroRNAs and gene network targeting VEGF: ADGRG1 (adhesion G protein-coupled receptor G1); calcifediol; FADS2 (fatty acid desaturase 2); FNDC3A (fibronectin type III domain containing 3A); FSH (follicle-stimulating hormone); Insulin; let-7a-5p (and other miRNAs w/seed GAGGUAG); MAP2K1/2; MEK1/2; MKK1/2; miR-125b-5p (and other miRNAs w/seed CCCUGAG); miR-126a-3p (and other miRNAs w/seed CGUACCG); mir-130; miR-155-5p (miRNAs w/seed UAAUGCU); miR-17-5p (and other miRNAs w/seed AAAGUGC); miR-185-5p (and other miRNAs w/seed GGAGAGA); miR-191-5p (and other miRNAs w/seed AACGGAA); miR-210-3p (miRNAs w/seed UGUGCGU); miR-23a-3p (and other miRNAs w/seed UCACAUU), miR-130a*; miR-26a-5p (and other miRNAs w/seed UCAAGUA); miR-1297; miR-30c-5p (and other miRNAs w/seed GUAAACA); mir-363; mir-423; miR-423-3p (miRNAs w/seed GCUCGGU); miR-432 (and other miRNAs w/seed CUUGGAG); miR-532-5p (and other miRNAs w/seed AUGCCUU), miR-6339; miR-92a-3p (and other miRNAs w/seed AUUGCAC), miR-25, miR-32, miR-363, miR-367; SLC38A1 (solute carrier family 38 member 1); Smad2/3 (TGF beta signaling proteins); SMAD6/7 (TGF beta signaling proteins); SYPL1 (synaptophysin like 1); TP53I11 (tumor protein p53 inducible protein 11); TUSC2 (tumor suppressor candidate 2); Vegf (VEGF mRNA). **C**: Inflammatory pathway - Recruitment and activation of eosinophils, Th2 lymphocytes, and macrophages: Histamine; IL-13 (interleukin-13); IL-4 (interleukin-4); IL-5 (interleukin-5); IL17A (interleukin-17A, CTLA-8); IL17B (interleukin-17B); Leukotrienes; TNFα (tumor necrosis factor α); VEGFA (vascular endothelial growth factor A).

post-transcriptional gene expression. MiRNA expression is necessary for cellular function, such as cell proliferation, apoptosis, inflammation, and a wide variety of cellular processes. MiRNAs function through base-pairing with mRNA, which leads to degradation or impaired translation of that particular mRNA [27]. Therefore, they can be referred to as "dimmer switches" for gene expression, because of their ability to repress gene expression without completely silencing it. Six of the miRNAs identified in the present study in primates exposed to ETS (let-7a, let-7c, miR-106a-5p, miR-106b-5p, miR-17-5p, and miR-361-5p) were also identified as circulatory candidate miRNAs in AMD [28-31]. The let-7 family and miR-361-5p are upregulated in retinal tissue in advanced AMD, targeting TGFBR1 [29,32]. MiR-17-5p has been shown to be upregulated in the plasma of patients with wet AMD [33]. MiR-17-5p negatively regulates TGFBR2 expression by directly binding to the 3′ untranslated region (UTR) of TGFBR2 mRNA, thus promoting cell growth and migration in cancer [34]. MiR-106 has been identified in a cohort of miRNAs that respond to oxidative stress exposure in ARPE-19 cells [35]. MiR-106a has been shown to target PTEN mRNA and lncRNA LINC00657, thus playing an important role in the regulation of PTEN expression in cancer [36].

Pathway analysis of dysregulated miRNAs after ETS exposure of Rhesus macaques targeted two signaling networks IL-17 and VEGF, and the inflammatory macrophage activation and recruitment pathway: Ingenuity Pathway Analysis of candidate miRNAs and their target genes identified two top networks that were activated during ETS exposure: IL-17A and VEGF. Upregulation of IL-17A has been previously observed with ETS exposure. Specifically, Siew and colleagues demonstrated that ETS increases bronchial mucosal IL-17A expression, and neutrophilic inflammation in asthmatics [37]. Levanen and colleagues implied that long-term exposure to tobacco smoke increases extracellular cytokine signaling via IL-17A in the peripheral airways of smokers with COPD and that this signaling may involve cytotoxic T-cells [38]. Interestingly, IL-17A also appears to be important in the pathogenesis of AMD. For example, genetic variants of IL-17A have been functionally associated with an increased risk of AMD [39]. Zhang and colleagues suggested that IL-17A triggers a key inflammatory mediator, IL-1β, in RPE cells, via NLRP3 inflammasome activation [40]. Therefore, the IL-17A pathway may be an important therapeutic target for AMD. Another study demonstrated that a functional single nucleotide polymorphism in the IL-17A 3′ UTR is targeted by miRNA in vitro and that miRNA-mediated gene dysregulation may play a role in the pathogenesis of AMD [41].

ETS exposure causes extensive tissue remodeling in the upper airways, and VEGF plays a critical role in this process. It has been shown that ETS extract has a stimulatory effect on VEGF expression through the TLR4/ROS/MAPKs/NF-kappaB signaling pathway in nasal fibroblasts [42]. In addition, a human RPE cell line (ARPE-19) exposed to an ETS concentrate resulted in premature senescence, thus supporting the role of oxidative damage in ETS-induced senescence activation. Furthermore, the senescent ARPE-19 cells upregulated VEGF and simultaneously downregulated complement factor H expression. As these phenomena are involved in AMD pathogenesis, these studies coupled with the present results support the hypothesis that ETS-induced senescence activation is important in the induction and progression of AMD. Moreover, this hypothesis would also explain the striking association of AMD pathogenesis with tobacco smoking [43].

One of the top IPA pathways that incorporates activation of both networks is the inflammatory recruitment and activation of eosinophils, Th2 lymphocytes, and macrophages pathway. This result fits with studies performed on infant monkeys after perinatal ETS exposure, which showed a statistically significant increase in mast cell, eosinophil, monocyte, and lymphocyte cell numbers in the lungs of infant monkeys [44]. It has been demonstrated that ETS exposure during early life enhances local Th2 immunity by impairing normal pulmonary Th1 immune maturation. This effect was greater in animals that began ETS exposure in utero compared to those that were exposed postnatal [45]. However, an association of the inflammatory response and two distinct types of immune responses—innate (complement system, phagocytes, mast cells, eosinophils, macrophages) and adaptive (T- and B-lymphocytes)—have been strongly implicated in AMD. An overactive complement system is associated with AMD pathogenesis, and serum proinflammatory cytokines, including IL-17, are elevated in patients with AMD. IL-17 is produced by complement C5a-receptor-expressing T-cells, such as gamma-delta T-cells, members of the innate immune response [46-48]. VEGF plays an important role in pathological angiogenesis, and anti-VEGF agents have been used to treat ocular diseases that are driven by pathological angiogenesis [49-51]. Based on the present results from the ETS-exposed monkeys and literature published on AMD, it appears likely that activation of IL-17A and VEGF networks, as well as inflammatory pathway of recruitment and activation of eosinophils, Th2 lymphocytes, and macrophages, are common for tobacco smoke and AMD pathogenesis.

In conclusion, this study identified changes in circulatory miRNAs in the plasma and ocular fluids of the Rhesus

macaque following ETS exposure, which differed markedly in comparison to age-related changes. The results of this study suggest that ETS exposure may be an appropriate animal model for early dry AMD. The identification and characterization of eye-specific miRNA in ocular tissue, as well as their target molecular pathways, will generate opportunities to identify novel strategies for therapeutic and environmental modulation or intervention for blinding ocular diseases.

APPENDIX 1. SUPPLEMENTARY TABLE 1. RHESUS MACAQUES IN THE STUDY.

To access the data, click or select the words "Appendix 1."

APPENDIX 2. SUPPLEMENTARY FIGURE 1

Spearman Rank Correlation of the signal values (**A, C, E**) between sample microarrays and Spearman Rank Correlation of the detection p values (**B, D, F**) between sample microarrays for plasma (**A,B**), vitreous (**C,D**), and aqueous (**E,F**). The heatmap contains a pairwise comparison of the signal values from all the selected sample microarray files, where the Spearman r2 values have been converted into a pseudocolor scale. To access the data, click or select the words "Appendix 2."

APPENDIX 3. SUPPLEMENTARY TABLE 2

Age-related gene expression changes in plasma of Rhesus macaques. To access the data, click or select the words "Appendix 3."

APPENDIX 4. SUPPLEMENTARY TABLE 3

Age-related gene expression changes in vitreous of Rhesus macaques. To access the data, click or select the words "Appendix 4."

APPENDIX 5. SUPPLEMENTARY TABLE 4

Age-related gene expression changes in aqueous of Rhesus macaques. To access the data, click or select the words "Appendix 5."

APPENDIX 6. SUPPLEMENTARY TABLE 5

Gene expression changes in plasma during ETS exposure of Rhesus macaques. To access the data, click or select the words "Appendix 6."

APPENDIX 7. SUPPLEMENTARY TABLE 6

Gene expression changes in vitreous during ETS exposure of Rhesus macaques. To access the data, click or select the words "Appendix 7."

ACKNOWLEDGMENTS

The authors are grateful to the CNPRC, the UC Davis Inhalation Exposure Core operators Louise Olsen, Chris Royer and Ross Allen, Dale Uyeminami from Environmental Health Center for nicotine exposure calculations, Kevin NH Nguyen for assisting with OCT scan readings, and Dr. Philip H. Kass, Professor Population Health & Reproduction, UC Davis, for mentoring ZW in statistical analysis. This project was funded by Barr Family Retina Research Foundation generous gift to the UC Davis Department of Ophthalmology (LSM, ZSM) and a pilot grant from the Environmental Health Center National Institute of Environmental Health Sciences P30ES023513 (ZSM) and NIH P30EY005722 (SF). The NEI Eye Core grant P30 EY012576 provided support for the tissue fixation, paraffin embedding and H&E staining. The CNPRC NIH P51OD011107 grant provided support for the colony and infrastructure, including the cores. The Affymetrix microRNA TitanChips 4.0 were processed through genomics services offered at the Institute for Human Genetics at UCSF.

REFERENCES

1. Velilla S, Garcia-Medina JJ, Garcia-Layana A, Dolz-Marco R, Pons-Vazquez S, Pinazo-Duran MD, Gomez-Ulla F, Arevalo JF, Diaz-Llopis M, Gallego-Pinazo R. Smoking and age-related macular degeneration: review and update. J Ophthalmol 2013; 2013:895147-[PMID: 24368940].

2. Olin KL, Morse LS, Murphy C, Paul-Murphy J, Line S, Bellhorn RW, Hjelmeland LM, Keen CL. Trace element status and free radical defense in elderly rhesus macaques (Macaca mulatta) with macular drusen. Proc Soc Exp Biol Med 1995; 208:370-7. [PMID: 7700885].

3. Lee JY, Chiu SJ, Srinivasan PP, Izatt JA, Toth CA, Farsiu S, Jaffe GJ. Fully automatic software for retinal thickness in eyes with diabetic macular edema from images acquired by cirrus and spectralis systems. Invest Ophthalmol Vis Sci 2013; 54:7595-602. [PMID: 24084089].

4. Slotkin TA, Pinkerton KE, Tate CA, Seidler FJ. Alterations of serotonin synaptic proteins in brain regions of neonatal Rhesus monkeys exposed to perinatal environmental tobacco smoke. Brain Res 2006; 1111:30-5. [PMID: 16876770].

5. Dwoskin LP, Teng L, Buxton ST, Crooks PA. (S)-(-)-Cotinine, the major brain metabolite of nicotine, stimulates nicotinic receptors to evoke [3H]dopamine release from rat striatal slices in a calcium-dependent manner. J Pharmacol Exp Ther 1999; 288:905-11. [PMID: 10027825].

6. Statistical Algorithms Description Document. Affymetrix. 2002.
7. Cruz-Gonzalez F, Cieza-Borrella C, Lopez Valverde G, Lorenzo-Perez R, Hernandez-Galilea E, Gonzalez-Sarmiento R. CFH (rs1410996), HTRA1 (rs112000638) and ARMS2 (rs10490923) gene polymorphisms are associated with AMD risk in Spanish patients. Ophthalmic Genet 2014; 35:68-73. [PMID: 23534868].
8. Francis PJ, Zhang H, Dewan A, Hoh J, Klein ML. Joint effects of polymorphisms in the HTRA1, LOC387715/ARMS2, and CFH genes on AMD in a Caucasian population. Mol Vis 2008; 14:1395-400. [PMID: 18682806].
9. Lee JGL, Orlan EN, Sewell KB, Ribisl KM. A new form of nicotine retailers: a systematic review of the sales and marketing practices of vape shops. Tob Control 2018; 27:e70-5. [PMID: 29208738].
10. McCausland K, Maycock B, Jancey J. The messages presented in online electronic cigarette promotions and discussions: a scoping review protocol. BMJ Open 2017; 7:e018633-[PMID: 29122804].
11. Aicher BO, Frishman WH. Electronic Cigarettes: Questions in the Mist. Cardiology 2016; in review[PMID: 27548689].
12. Polverino F, Doyle-Eisele M, McDonald J, Wilder JA, Royer C, Laucho-Contreras M, Kelly EM, Divo M, Pinto-Plata V, Mauderly J, Celli BR, Tesfaigzi Y, Owen CA. A novel nonhuman primate model of cigarette smoke-induced airway disease. Am J Pathol 2015; 185:741-55. [PMID: 25542772].
13. Curtis JL, Freeman CM. Why do we need a nonhuman primate model of smoking-induced COPD? Am J Pathol 2015; 185:610-3. [PMID: 25576784].
14. Raghuveer G, White DA, Hayman LL, Woo JG, Villafane J, Celermajer D, Ward KD, de Ferranti SD, Zachariah J. American Heart Association Committee on Atherosclerosis H, Obesity in the Young of the Council on Cardiovascular Disease in the Y, Behavior Change for Improving Health Factors Committee of the Council on L, Cardiometabolic H, Council on E, Prevention, Stroke C. Cardiovascular Consequences of Childhood Secondhand Tobacco Smoke Exposure: Prevailing Evidence, Burden, and Racial and Socioeconomic Disparities: A Scientific Statement From the American Heart Association. Circulation 2016; 134:e336-59. [PMID: 27619923].
15. Palacios N. Air pollution and Parkinson's disease - evidence and future directions. Rev Environ Health 2017; 32:303-313. [PMID: 28731859].
16. Niemann B, Rohrbach S, Miller MR, Newby DE, Fuster V, Kovacic JC. Oxidative Stress and Cardiovascular Risk: Obesity, Diabetes, Smoking, and Pollution: Part 3 of a 3-Part Series. J Am Coll Cardiol 2017; 70:230-51. [PMID: 28683970].
17. Florescu A, Ferrence R, Einarson T, Selby P, Soldin O, Koren G. Methods for quantification of exposure to cigarette smoking and environmental tobacco smoke: focus on developmental toxicology. Ther Drug Monit 2009; 31:14-30. [PMID: 19125149].
18. Jarvis MJ, Fidler J, Mindell J, Feyerabend C, West R. Assessing smoking status in children, adolescents and adults: cotinine cut-points revisited. Addiction 2008; 103:1553-61. [PMID: 18783507].
19. Ayhan Z, Kaya M, Ozturk T, Karti O, Hakan Oner F. Evaluation of Macular Perfusion in Healthy Smokers by Using Optical Coherence Tomography Angiography. Ophthalmic Surg Lasers Imaging Retina 2017; 48:617-22. [PMID: 28810036].
20. Dervisogullari MS, Totan Y, Tenlik A, Yuce A, Guler E. Effect of smoking on retina nerve fiber layer and ganglion cell-inner plexiform layer complex. Cutan Ocul Toxicol 2015; 34:282-5. [PMID: 25363066].
21. Demirci S, Gunes A, Demirci S, Kutluhan S, Tok L, Tok O. The effect of cigarette smoking on retinal nerve fiber layer thickness in patients with migraine. Cutan Ocul Toxicol 2016; 35:21-5. [PMID: 25597373].
22. El-Shazly AAE, Farweez YAT, Elewa LS, Elzankalony YA, Farweez BAT. Effect of Active and Passive Smoking on Retinal Nerve Fibre Layer and Ganglion Cell Complex. J Ophthalmol 2017; 2017:6354025-[PMID: 28491470].
23. Espinosa-Heidmann DG, Suner IJ, Catanuto P, Hernandez EP, Marin-Castano ME, Cousins SW. Cigarette smoke-related oxidants and the development of sub-RPE deposits in an experimental animal model of dry AMD. Invest Ophthalmol Vis Sci 2006; 47:729-37. [PMID: 16431974].
24. Lujan BJ, Roorda A, Knighton RW, Carroll J. Revealing Henle's fiber layer using spectral domain optical coherence tomography. Invest Ophthalmol Vis Sci 2011; 52:1486-92. [PMID: 21071737].
25. Rubio M, Bustamante M, Hernandez-Ferrer C, Fernandez-Orth D, Pantano L, Sarria Y, Pique-Borras M, Vellve K, Agramunt S, Carreras R, Estivill X, Gonzalez JR, Mayor A. Circulating miRNAs, isomiRs and small RNA clusters in human plasma and breast milk. PLoS One 2018; 13:e0193527-[PMID: 29505615].
26. He Y, Deng F, Yang S, Wang D, Chen X, Zhong S, Zhao J, Tang J. Exosomal microRNA: a novel biomarker for breast cancer. Biomarkers Med 2018; 12:177-88. [PMID: 29151358].
27. Sonkoly E, Pivarcsi A. microRNAs in inflammation. Int Rev Immunol 2009; 28:535-61. [PMID: 19954362].
28. Berber P, Grassmann F, Kiel C, Weber BH. An Eye on Age-Related Macular Degeneration: The Role of MicroRNAs in Disease Pathology. Mol Diagn Ther 2017; 21:31-43. [PMID: 27658786].
29. Ren C, Liu Q, Wei Q, Cai W, He M, Du Y, Xu D, Wu Y, Yu J. Circulating miRNAs as Potential Biomarkers of Age-Related Macular Degeneration. Cell Physiol Biochem 2017; 41:1413-23. [PMID: 28315863].
30. Menard C, Rezende FA, Miloudi K, Wilson A, Tetreault N, Hardy P, SanGiovanni JP, De Guire V, Sapieha P. MicroRNA signatures in vitreous humour and plasma of patients with exudative AMD. Oncotarget 2016; 7:19171-84. [PMID: 27015561].

31. Szemraj M, Bielecka-Kowalska A, Oszajca K, Krajewska M, Gos R, Jurowski P, Kowalski M, Szemraj J. Serum MicroRNAs as Potential Biomarkers of AMD. Med Sci Monit 2015; 21:2734-42. [PMID: 26366973].

32. Grassmann F, Schoenberger PG, Brandl C, Schick T, Hasler D, Meister G, Fleckenstein M, Lindner M, Helbig H, Fauser S, Weber BH. A circulating microrna profile is associated with late-stage neovascular age-related macular degeneration. PLoS One 2014; 9:e107461-[PMID: 25203061].

33. Ertekin S, Yildirim O, Dinc E, Ayaz L, Fidanci SB, Tamer L. Evaluation of circulating miRNAs in wet age-related macular degeneration. Mol Vis 2014; 20:1057-66. [PMID: 25221421].

34. Qu Y, Zhang H, Duan J, Liu R, Deng T, Bai M, Huang D, Li H, Ning T, Zhang L, Wang X, Ge S, Zhou L, Zhong B, Ying G, Ba Y. MiR-17–5p regulates cell proliferation and migration by targeting transforming growth factor-beta receptor 2 in gastric cancer. Oncotarget 2016; 7:33286-96. [PMID: 27120811].

35. Ayaz L, Dinc E. Evaluation of microRNA responses in ARPE-19 cells against the oxidative stress. Cutan Ocul Toxicol 2017; 37:1-6. [PMID: 28707489].

36. Hu B, Cai H, Zheng R, Yang S, Zhou Z, Tu J. Long non-coding RNA 657 suppresses hepatocellular carcinoma cell growth by acting as a molecular sponge of miR-106a-5p to regulate PTEN expression. Int J Biochem Cell Biol 2017; 92:34-42. [PMID: 28919047].

37. Siew LQ, Wu SY, Ying S, Corrigan CJ. Cigarette smoking increases bronchial mucosal IL-17A expression in asthmatics, which acts in concert with environmental aeroallergens to engender neutrophilic inflammation. Clin Exp Allergy 2017; 47:740-50. [PMID: 28211191].

38. Levanen B, Glader P, Dahlen B, Billing B, Qvarfordt I, Palmberg L, Larsson K, Linden A. Impact of tobacco smoking on cytokine signaling via interleukin-17A in the peripheral airways. Int J Chron Obstruct Pulmon Dis 2016; 11:2109-16. [PMID: 27660428].

39. Zhang S, Liu Y, Lu S, Cai X. Genetic variants of interleukin 17A are functionally associated with increased risk of age-related macular degeneration. Inflammation 2015; 38:658-63. [PMID: 25028103].

40. Zhang S, Yu N, Zhang R, Zhang S, Wu J. Interleukin-17A Induces IL-1beta Secretion From RPE Cells Via the NLRP3 Inflammasome. Invest Ophthalmol Vis Sci 2016; 57:312-9. [PMID: 26830368].

41. Popp NA, Yu D, Green B, Chew EY, Ning B, Chan CC, Tuo J. Functional single nucleotide polymorphism in IL-17A 3′ untranslated region is targeted by miR-4480 in vitro and may be associated with age-related macular degeneration. Environ Mol Mutagen 2016; 57:58-64. [PMID: 26765636].

42. Shin JM, Park JH, Kim HJ, Park IH, Lee HM. Cigarette smoke extract increases vascular endothelial growth factor production via TLR4/ROS/MAPKs/NF-kappaB pathway in nasal fibroblast. Am J Rhinol Allergy 2017; 31:78-84. [PMID: 28452703].

43. Marazita MC, Dugour A, Marquioni-Ramella MD, Figueroa JM, Suburo AM. Oxidative stress-induced premature senescence dysregulates VEGF and CFH expression in retinal pigment epithelial cells: Implications for Age-related Macular Degeneration. Redox Biol 2016; 7:78-87. [PMID: 26654980].

44. Yu M, Zheng X, Peake J, Joad JP, Pinkerton KE. Perinatal environmental tobacco smoke exposure alters the immune response and airway innervation in infant primates. J Allergy Clin Immunol 2008; 122:640-7. [PMID: 18571708].

45. Wang L, Joad JP, Zhong C, Pinkerton KE. Effects of environmental tobacco smoke exposure on pulmonary immune response in infant monkeys. J Allergy Clin Immunol 2008; 122:400-6. [PMID: 18502491].

46. Coughlin B, Schnabolk G, Joseph K, Raikwar H, Kunchithapautham K, Johnson K, Moore K, Wang Y, Rohrer B. Connecting the innate and adaptive immune responses in mouse choroidal neovascularization via the anaphylatoxin C5a and gammadeltaT-cells. Sci Rep 2016; 6:23794-[PMID: 27029558].

47. Zhao Z, Liang Y, Liu Y, Xu P, Flamme-Wiese MJ, Sun D, Sun J, Mullins RF, Chen Y, Cai J. Choroidal gammadelta T cells in protection against retinal pigment epithelium and retinal injury. FASEB J 2017; 31:4903-16. [PMID: 28729290].

48. Zhao Z, Xu P, Jie Z, Zuo Y, Yu B, Soong L, Sun J, Chen Y, Cai J. gammadelta T cells as a major source of IL-17 production during age-dependent RPE degeneration. Invest Ophthalmol Vis Sci 2014; 55:6580-9. [PMID: 25212781].

49. Nakahara T, Morita A, Yagasaki R, Mori A, Sakamoto K. Mammalian Target of Rapamycin (mTOR) as a Potential Therapeutic Target in Pathological Ocular Angiogenesis. Biol Pharm Bull 2017; 40:2045-9. [PMID: 29199229].

50. Farnoodian M, Wang S, Dietz J, Nickells RW, Sorenson CM, Sheibani N. Negative regulators of angiogenesis: important targets for treatment of exudative AMD. Clin Sci 2017; 131:1763-80. [PMID: 28679845].

51. Al-Zamil WM, Yassin SA. Recent developments in age-related macular degeneration: a review. Clin Interv Aging 2017; 12:1313-30. [PMID: 28860733].

Articles are provided courtesy of Emory University and the Zhongshan Ophthalmic Center, Sun Yat-sen University, P.R. China. The print version of this article was created on 24 September 2018. This reflects all typographical corrections and errata to the article through that date. Details of any changes may be found in the online version of the article.